ARTICLE TYPE www.rsc.org/xxxxxx | XXXXXXXX

Enzymeless multi-sugar fuel cells with high power output based on 3D graphene-Co_3O_4 hybrid electrodes†

Yun Chen, Kenath Priyanka Prasad, Xuewan Wang, Hongchang Pang, Ruyu Yan, Aung Than, Mary B. Chan-Park, Peng Chen*

Received (in XXX, XXX) Xth XXXXXXXXX 200X, Accepted Xth XXXXXXXXX 200X
First published on the web Xth XXXXXXXXX 200X
DOI: 10.1039/b000000x

Biofuel cells (BFCs), which use enzymes as the catalysts to harvest energy from green and sustainable fuels abundantly producible from biological systems, are promising next-generation energy devices. But the poor stability and high specificity to only one fuel type of these bio-catalysts largely limit the practice use of current BFCs. In this contribution, we demonstrate a unique fuel cell which, equipped with two identical enzyme-free electrodes based on Co_3O_4 coated 3D graphene, is able to efficiently harvest electricity from various sweet biofuels (glucose, sucrose, or lactose). Taking advantages of the dual catalytic ability of nanostructured Co_3O_4 for both glucose oxidation and oxygen reduction as well as the exceptional electrical and structural properties of 3D graphene, our glucose-powered fuel cell, with good long-term stability, offers high open circuit voltage (~1.1 V) and power density output (2.38 ± 0.17 mW cm^{-2}).

1. Introduction

The continuously accelerated consumption of the traditional non-renewable energy makes it ever urgent for researchers to find replaceable new power sources allowing conversion of chemical energy into electrical energy. Biofuel cells (BFCs) are promising next-generation energy devices which are able to use enzymes or microorganisms as catalysts to harvest energy from green and sustainable fuels producible from biological systems in gentle and environmental-friendly conditions.[1-5]

Most enzymatic BFCs use glucose as the biofuel due to its vast abundance, readily availability, and green chemistry. And as glucose is a universal energy currency in living beings, glucose based BFC is a potential power source for bionic implants.[3, 6-8] Current glucose-based BFCs, however, rely on glucose specific enzymes, namely, glucose oxidase (GOD) and glucose dehydrogenase (GDH), to oxidize glucose molecules at the anode. To complete the circuit, usually oxygen (O_2) is reduced at the cathode by another enzyme, laccase or bilirubin oxidase (BOD). However, the poor stability of the bioenzymes largely limits the practical use of BFCs,[1, 2] and the high specificity of these enzymes excludes the utilization of other biofuels (e.g., other sugars) also available in the biomasses or biofluids. Furthermore, non-ideal coupling between enzymes and electrodes compromises the BFC performance. Redox mediators are often required in a BFC to facilitate electron transfer from the embedded catalytic center of the enzyme to the electrode.[1-3, 9] These mediators are sometimes toxic and unstable,[1, 3] and indirect electron transfer through mediators sacrifices open circuit voltage (OCV),[3] thus the power output. Therefore, it is imperative to overcome these current problems of enzymatic BFCs.

Nanostructured materials (e.g., nanoparticles of precious metals or metal oxides) which exhibit exceptional catalytic properties provide novel, stable, and efficient alternatives to bioenzymes.[10-12] Among them, cobalt oxides (Co_3O_4) have attracted widespread attention for various applications due to its extraordinary electrochemical and catalytic properties.[13-15] Recently, the excellent catalytic ability of Co_3O_4 nanostructures towards glucose oxidation has been demonstrated and exploited for enzyme-free glucose detection.[16-18] This implies the possibility of using nanostructured Co_3O_4 as a low-cost and stable substitution to glucose enzymes. However, just like other metal oxides, Co_3O_4 is poorly conductive. Therefore, it needs to be functionalized onto or hybridized with conductive materials in order to construct an active and conductive electrode. Owing to its extraordinarily high conductivity, specific surface area and chemical inertness, graphene (one-atom-thick crystalline carbon sheet) is a new and attractive electrode material to provide support for catalysts and pathways for electron transfer/conduction.[19-22] But compositing other nanomaterials with small individual graphene sheets often suffer from the problems, such as, aggregation, reduced conductivity, compromised surface area, and poor infiltration. Recently, 3D architectures of 2D graphene have been demonstrated, and used as novel 3D electrodes for various applications taking advantages of its high conductivity, large surface area, and macroporous structure.[23-28]

In this study, Co_3O_4 hybridized 3D graphene electrodes are fabricated as both the anode for glucose oxidation and the cathode for oxygen reduction (Scheme 1). Such enzyme and mediator-free fuel cell (FC) offers high open circuit voltage (~1.1

Division of Bioengineering, School of Chemical and Biomedical Engineering, Nanyang Technological University, 70 Nanyang Drive, 637457, Singapore. Fax: +65 67911761; Tel: +65 65141086
**E-mail: chenpeng@ntu.edu.sg*

† Electronic supplementary information (ESI) available. See DOI: 10.1039/b000000x/

Volts, close to the theoretical limit), high power output (2.38 ± 0.17 mW cm^{-2}), and good long-term stability (only ~27% run-down after 30 days). Moreover, we demonstrate that this FC is able to use other sugar fuels as well (sucrose and lactose).

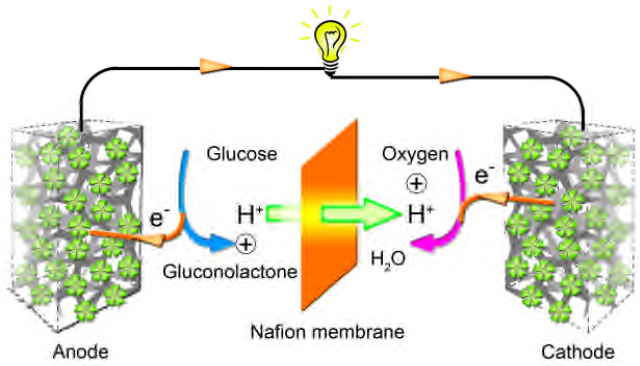

Scheme 1. Illustration of the glucose-powered FC based on 3D graphene-Co_3O_4 anode and cathode.

2. Experimental

2.1 Fabrication of 3D graphene and 3D graphene-Co_3O_4 hybrid electrodes

As reported previously, 3D graphene was synthesized by chemical vapor deposition (CVD) under atmospheric pressure using nickel foam (Alantum Advanced Technology Materials, China) as the substrate and ethanol as the carbon source.[24, 29, 30] Nickel foam was then etched away in 3M HCl leaving 3D graphene foam free-standing. Subsequently, with $Co(NO_3)_2{\cdot}6H_2O$ solution (0.1 M) as the electrolyte, $Co(OH)_2$ nanostructures were electrochemically deposited onto bare 3D graphene by applying a constant potential of -1.0 V (*vs.* Ag/AgCl reference electrode) for 800 s. After thorough rinsing with DI-water, the 3D graphene-Co_3O_4 hybrid was annealed at 400 °C for 4 h to transform $Co(OH)_2$ to Co_3O_4. Finally, the obtained 3D graphene-Co_3O_4 foam (~0.7 × 0.8 cm, 0.5 mm thick) was mounted onto a glass slide, and an electrical lead was made by silver paint and copper wire insulated with silicone rubber.

2.2 Chemicals and solutions

All chemicals were purchased from Sigma-Aldrich. The sugar stock solutions (1 M) were prepared at least 24 h before use. pH 5.0 buffer solution (0.2 M) was made of sodium acetate and acetic acid; pH 7.0 buffer (0.2 M) was made of NaH_2PO_4 and Na_2HPO_4; pH 11.0 solution (0.2 M) was freshly prepared with NaOH and NaCl.

2.3 Material characterizations and electrochemical measurements

Field emission scanning electron microscope (FESEM, JMS-6700F), confocal Raman system (WITec CRM200 using 488 nm laser), and X-ray diffraction (XRD) system (Bruker D8 Avance diffractometer using Cu Kα radiation) were used to characterize our samples. Contact angles were examined with a FTA200 Dynamic Contact Angle Analyzer. Electrochemical measurements were performed using an electrochemical workstation (CHI 660D). Cyclic voltammetric (CV) measurements were conducted with a three-electrode cofiguration including a Pt wire as the counter electrode, a saturated calomel electrode (SCE) as the reference electrode, and a 3D graphene-Co_3O_4 hybrid electrode as the working electrode. The open circuit potential of the electrode was determined with a two-electrode configuration (SCE as the reference).

2.4 Fuel cell design and test

The FC house-made with acrylic glass was divided into the anodic and cathodic compartments by a proton exchange film (perfluorosulfonic acid/PTFE copolymer membrane, DuPont™ Nafion®, 25.4 μm thick). The anodic chamber was filled with nitrogen-saturated buffer solution containing different kinds of fuels (sugars) at defined concentrations while the cathodic chamber was filled with oxygen-saturated buffer solution. The open circuit voltage (E^{ocv}) was continuously monitored by CHI-660D electrochemical station after assembling of the FC. Once E^{ocv} reached the steady-state, FC was loaded with various external resistance (100 Ω ~ 100 kΩ) and the corresponding output voltages were recorded with a precision digital multimeter. These results were used to determine the polarization curves and the power density curves.

3. Results and discussion

3.1 Material Characterizations

The structure and surface morphology of the bare 3D graphene and 3D graphene-Co_3O_4 hybrid were investigated by FESEM. As shown in Fig. 1A, 3D graphene exhibits a monolithic macroporous structure (pore size of ~200 μm). After electrochemical deposition, a continuous and regular layer of flower-like Co_3O_4 nanostructure forms around the 3D graphene scaffold (Fig. 1B). In the Raman spectrum depicted in Fig. 1C, the absence of D band (at ~1350 cm^{-1}) and the ratio between G (1584 cm^{-1}) and 2D (2710 cm^{-1}) peaks suggest that the 3D graphene is defect-free and mainly few-layered.[23, 26] In comparison, the Raman spectrum of 3D graphene-Co_3O_4 hybrid manifests additional peaks at 487, 532, 621, and 694 cm^{-1}, corresponding to E_g, F_{2g}^1, F_{2g}^2, and A_g^1 modes of crystalline Co_3O_4, respectively.[17] The XRD pattern of 3D graphene gives two characteristic diffraction peaks at 26.5° and 54.6° (2θ) due to the (002) and (004) reflections of graphitic carbon, respectively (Fig. 1D). In addition to these graphitic peaks, the 3D graphene-Co_3O_4 hybrid shows ten diffraction peaks resulted from the (111), (220), (311), (222), (400), (422), (511), (440), (531) and (620) planes of crytalline Co_3O_4.[13, 17] Both Raman and XRD characterizations indicate the success deposition of Co_3O_4 with high crystallinity on defect-free graphene. Furthermore, the contact angle measurement suggests that the Co_3O_4 coating renders the highly hydrophobic bare 3D graphene hydrophilic (Fig. 1E). This ensures that the electrolyte can easily and fully penetrate into the 3D electrode (optical image shown in Fig. 1F).

As shown in Fig. S1 in Electronic Supplementary Information (ESI), the morphology of deposited Co_3O_4 microflowers evolves with the electrochemical deposition duration, it reaches almost full blossom when the deposition duration is increased to 800 s. In all the following experiments, we use electrodes with 800s electrochemical deposition of Co_3O_4 (same as shown in Fig. 1B

inset) because the open circuit potential of such electrodes reaches its maximum while the electrodes using less deposition time delivers lower open circuit potential.

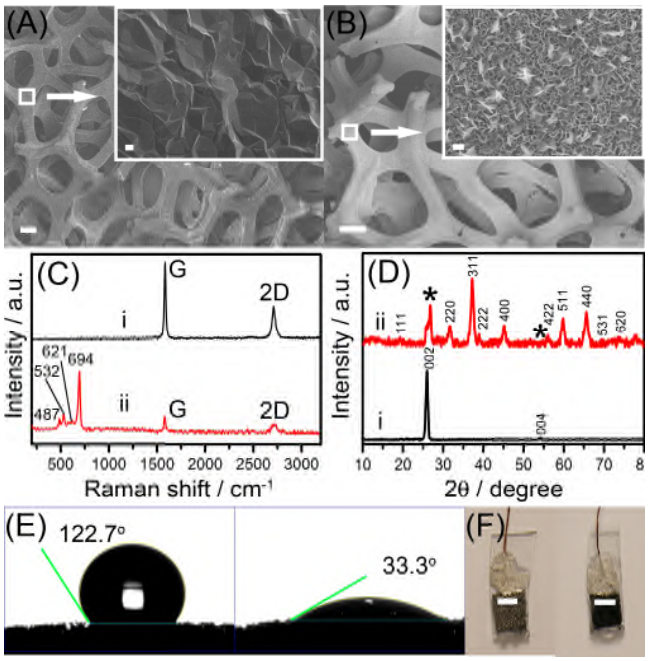

Fig. 1. (A and B) FESEM images of bare 3D graphene (A) and 3D graphene-Co_3O_4 hybrid (B) (scale bar = 100 μm). Each inset shows the skeleton surface of the sample (scale bar = 1 μm). (C) Raman spectra and (D) XRD spectra of 3D graphene (i) and 3D graphene-Co_3O_4 hybrid (ii). In D, * marks the signal from 3D graphene. (E) Contact angle of 3D graphene (left) and 3D graphene-Co_3O_4 hybrid (right). (F) Optical images of the 3D graphene electrode before (left) and after (right) deposition of Co_3O_4. Scale bar = 0.5 cm.

3.2 The anodic properties

Serving as the anode, the open circuit potential (E_a^{ocp}) of 3D hybrid electrode is measured at acidic (pH 5.0), neutral (pH 7.0), and basic (pH 11.0) conditions (Fig. 2A). As expected, without glucose, the steady-steady E_a^{ocp} is essentially zero (0.048 ± 0.021 V, n = 3). Interestingly, in the presence of glucose (200 mM), E_a^{ocp} is the maximum at the acidic condition (-0.591 ± 0.012 V, n = 3), in comparison to E_a^{ocp} at the neutral (-0.538 ± 0.009 V, n = 3) and at basic conditions (-0.261 ± 0.025 V, n = 3). E_a^{ocp} at the acidic condition essentially reaches the theoretical thermodynamic equilibrium potential of the gluconolactone/ glucose couple at pH 5.0 (φ' = -0.57 V *vs.* SCE),[31] suggesting that the nanostructured Co_3O_4 acts as a perfect catalyst to oxidize glucose (glucose → gluconolactone + $2H^+$ + $2e^-$). To the best of our knowledge, the previously reported anodes based on glucose-specific enzymes (GOD or GDH) are not able to reach this ideal E_a^{ocp}. Not to mention that, enzymes are not stable and expensive.

To understand the reason for optimal operation in the acidic condition, cyclic voltammogram (CV) of the electrode was conducted. The CV obtained at pH 5.0 without glucose (Fig. 2B) shows two oxidation peaks. Co_3O_4 (sometimes written as $CoO.Co_2O_3$) is a mixed valence compound containing both Co^{II} and Co^{III} oxidation states. The lower oxidation peak (at ~0.31 V) is probably ascribed to the oxidation of Co^{II} to Co^{III} in the following reaction:

$$2Co_3O_4 + H_2O \leftrightarrow 3Co_2O_3 + 2H^+ + 2e^- \qquad (1)$$

while the higher oxidation peak (at ~0.56 V) is likely due to the oxidation of Co^{III} to Co^{IV} as formulated below:

$$Co_2O_3 + H_2O \leftrightarrow 2CoO_2 + 2H^+ + 2e^- \qquad (2)$$

It is known that both Co^{III} and Co^{IV} have strong oxidative ability while converting to Co^{II} and Co^{III}, respectively.[32, 33] In acidic conditions, the theoretical equilibrium potentials of Co^{III} to Co^{II} conversion (φ' = 0.48 V *vs.* SCE) and Co^{IV} to Co^{III} conversion (φ' = 0.909 V) are high, suggesting their strong ability to oxidize glucose. In the presence of glucose, Co^{IV} and Co^{III} would be more readily reduced to Co^{II} whereby promoting reaction (1) and (2). As the consequence, both oxidation peaks increase while the reduction peak (at ~0.271 V) disappears with addition of 1 mM glucose (Fig. 2B). However, it should be pointed out that only Co^{III} exists in the native state of Co_3O_4, and is responsible for the open circuit potential.

In basic conditions, Co_3O_4 electrocatalyzes glucose in a different way as previously reported.[17, 18] The two electro-oxidation reactions (at the two oxidation peaks) are given as follows:

$$Co_3O_4 + OH^- + H_2O \leftrightarrow 3CoOOH + e^- \qquad (3)$$

$$CoOOH + OH^- \leftrightarrow CoO_2 + H_2O + e^- \qquad (4)$$

The thermodynamic equilibrium potentials of Co^{III} to Co^{II} conversion (φ' = 0.140 V) and Co^{IV} to Co^{III} conversion (φ' = 0.480 V) are significantly lower as compared with those in acidic conditions,[34, 35] suggesting that the oxidative ability of high valence Co is compromised by high pH. In support of this, it is observed that glucose induced increase of the oxidation current at the lower potential peak (Co^{III} as the catalyst) vanishes while the increase at the higher potential (Co^{IV} as the catalyst) is much less as compared with that in the acidic condition (231 ± 10 μA cm^{-2}, n = 3 *vs.* 469 ± 37 μA cm^{-2}, n = 3) (Fig. 2D). Not surprisingly, the CV obtained in neutral condition demonstrates the insignificant oxidative ability of Co^{III} and moderate oxidative ability of Co^{IV} (Fig. 2C).

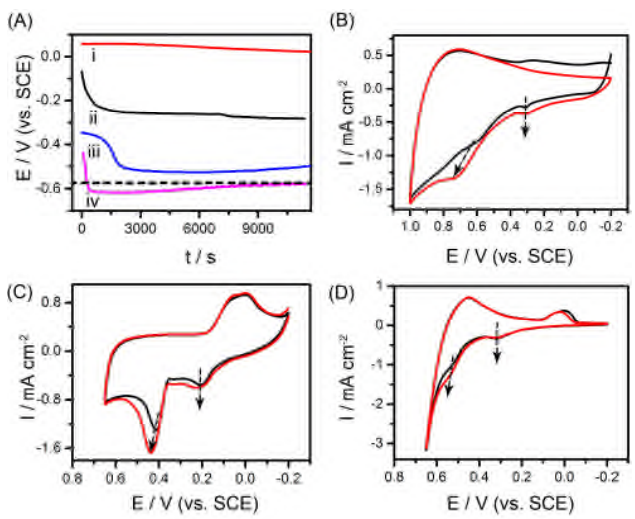

Fig. 2. (A) The open circuit potential of the 3D graphene-Co_3O_4 anode in pH 5.0 electrolyte solution without glucose (i), pH 11.0 electrolyte with glucose (200 mM) (ii), pH 7.0 electrolyte with glucose (iii), and pH 5.0

electrolyte with glucose (iv). The dashed-line indicates the theoretical limit. (B-D) The CVs of the hybrid electrode without (black) or with (red) glucose (1 mM), in pH 5.0 (B), pH 7.0 (C), or pH 11.0 electrolyte (D). The dashed-arrows indicate the changes of oxidation peaks; and all solutions were saturated with nitrogen.

The native Co_3O_4 contains both Co^{III} and Co^{II}. We further demonstrate that the CoOOH (containing only Co^{III}) coated 3D graphene was able to produce a significant E_a^{ocp} of -0.587 ± 0.049 V (n = 3) resulting from glucose oxidation whereas $Co(OH)_2$ (Co^{II} only) coated 3D graphene electrode could not give an appreciable E_a^{ocp} (Fig. S2 and S3 in the ESI). This experiment suggests that it is the strong oxidative ability of Co^{III} (not Co^{II}) in Co_3O_4 (particularly in acidic condition) responsible for the high anodic E_a^{ocp}.

3.3 The cathodic properties

Co^{II}, which has been shown to possess reducing ability (towards, e.g., oxygen and H_2O_2) due to Co^{II} to Co^{III} conversion,[36] equally co-exists in Co_3O_4, implying that the same 3D graphene-Co_3O_4 electrode may also be able to serve as the FC cathode. The open circuit potentials (E_c^{ocp}) of the 3D graphene-Co_3O_4 cathode, which is resulted from the reaction: $O_2 + 4H^+ + 4e^- \rightarrow 2H_2O$, were measured at acidic (pH 5.0), neutral (pH 7.0) and basic conditions (pH 11.0), with saturated oxygen. As shown in Fig. 3A, like the anodic potential E_a^{ocp}, E_c^{ocp} is also most significant in the acidic condition (0.520 ± 0.010 V, n = 3), in contrast to E_c^{ocp} at neutral (0.312 V ± 0.014 V, n = 3) and basic (0.056 ± 0.009 V, n = 3) electrolyte. And this value is comparable to the theoretical equilibrium potential (φ' = +0.637 V *vs.* SCE) of the O_2/H_2O couple at pH 5.0.[31]

The optimal performance in the acidic condition is not unexpected because the oxidative capability of O_2 decreases with the increasing pH because of the decreasing φ' (0.637 V at pH 5.0, 0.519 V at pH 7.0, and 0.164 V at pH 11.0).[31] To further investigate this phenomenon, the CVs were obtained at the different pH levels.

In the acidic conditions, the reduction peak in the CV (Fig. 3B) is attributed to the following reaction:[37]

$$Co_3O_4 + 2H^+ + 2e^- \leftrightarrow 3CoO + H_2O \quad (5)$$

Obviously, this reaction is favoured at a low pH. φ' of this reaction at pH 5.0 (0.239 V *vs.* SCE) is significantly lower than that of oxygen reduction (0.637 V), indicating the good catalytic ability of Co^{II} to Co^{III} conversion to oxygen reduction. In agreement with this view, the introduction of oxygen largely increases the reduction current (Fig. 3B). In basic conditions, the reduction peak in the CV is resulted from the reaction below:[37]

$$Co_3O_4 + 4H_2O + 2e^- \leftrightarrow 3Co(OH)_2 + 2OH^- \quad (6)$$

The equilibrium potential φ' of this reaction at pH 11.0 (0.810 V *vs.* SCE) which is higher than φ' of oxygen reduction (0.164 V), indicating that in a basic condition Co^{II} loses its ability to reduce oxygen. Consequently, the introduction of oxygen fails to enhance the reduction current in the CV as shown in Fig. 3D. Consistently, the reducing ability of Co^{II} is moderate in the neutral condition as compared to that in the acidic condition (125 ± 9 μA cm^{-2} *vs.* 162 ± 10 μA cm^{-2} as the oxygen-enhanced reduction current, n = 3).

We further show that the $Co(OH)_2$ coated 3D graphene electrode offered a large E_c^{ocp} of 0.543 ± 0.020 V (n=3) whereas CoOOH coated 3D graphene electrode only produced a trivial E_a^{ocp}, indicating the reducing ability of Co^{II} (but not Co^{III}) to oxygen (Fig. S3 in the ESI). Together with the results demonstrated in the previous section, it can be concluded that the dual catalytic ability of Co_3O_4 (thus its ability to serve as both BFC anode and cathode) is due to the strong oxidative ability of Co^{III} to glucose and the excellent reducing ability of Co^{II} to oxygen.

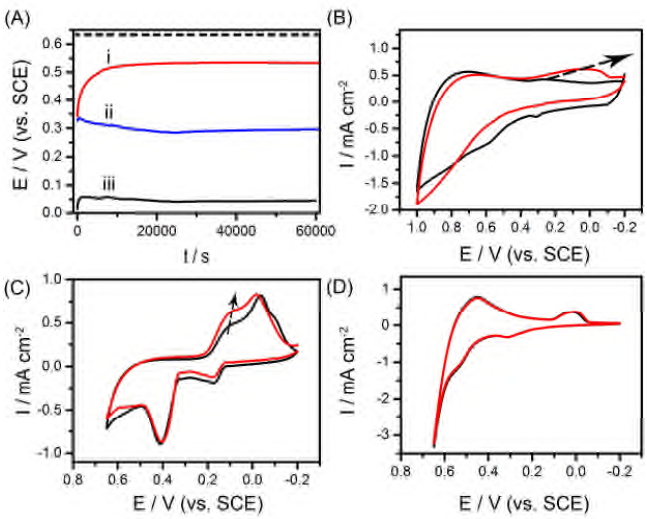

Fig. 3. (A) The open circuit potential of the 3D graphene-Co_3O_4 hybrid cathode in pH 5.0 (i), pH 7.0 (ii), or pH 11.0 (iii) electrolyte solution saturated with oxygen. The dashed-line indicates the theoretical limit. (B-D) The CVs of the hybrid electrode, with saturation of nitrogen (black) or saturation of oxygen (red), in pH 5.0 (B), pH 7.0 (C), or pH 11.0 (D) electrolyte solution. The dashed-arrows indicate the changes of reduction peaks.

3.4 The performance of the sugar-powered fuel cell

The fuel cell (FC) equipped with both 3D graphene-Co_3O_4 anode and cathode works as illustrated in Scheme 1. At the anode, Co^{III} sites in the Co_3O_4 nanostructures efficiently catalyze glucose oxidation *via* its conversion to Co^{II}; the thereby obtained electrons are rapidly conducted away by the 3D-multiplexed conductive highways of the graphene foam to the cathode leading to restoration of the converted Co^{II} back to Co^{III} state; at the cathode, the Co^{II} sites of Co_3O_4 layer reduce oxygen *via* its conversion to the higher valence states (Co^{III} or Co^{IV}) which soon return to the divalent state while receiving electrons from the anode; Co^{III} sites at the cathode may promote chemisorption of O_2 molecules through their cationic d-orbitals;[38] to complete the circuit, the current in the solution is carried by the proton flux from the anode to the cathode. The generated electricity will last as long as the fuel molecules (glucose and oxygen) are not depleted.

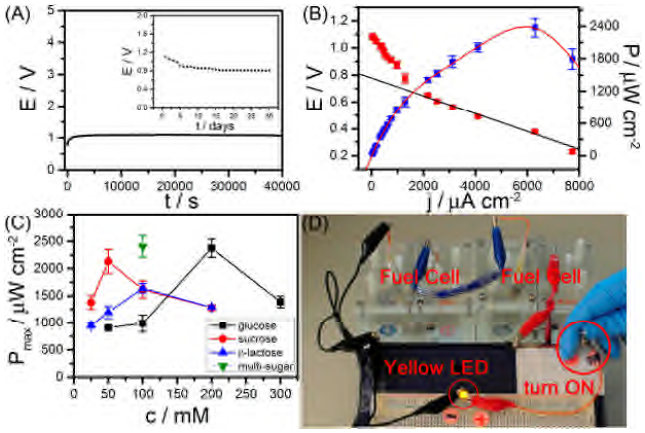

Fig. 4 (A) The open circuit voltage from one FC. Inset shows the open circuit voltage from one cell over 30 days. (B) Polarization curve and power output curve of the FC. The black line is the fitting of the linear region of the polarization curve. (C) The maximum power output at different concentrations of glucose, sucrose or β-lactose or their mixture (50 mM glucose, 25 mM sucrose, and 25 mM β-lactose). (D) The device image showing a yellow LED powered by two FC in series. In (B) and (C), all data points are the average from three independent experiments and the error bars indicate the standard deviation.

Our FCs are operated in the desired acidic condition (pH 5.0). As shown in Fig. 4A, in the presence of 200 mM glucose, the open circuit voltage of the FC (E_{cell}^{ocv}) is ~1.1 V which is close to the theoretical limit of 1.2 V. Two FCs in series give an E_{cell}^{ocv} of ~2.1 V. Such E_{cell}^{ocv} outperforms all the previously reported enzymatic BFCs (Table 1), including the recent one using carbon nanotubes as the electrode material.[39] Our enzyme- and mediator-free FC is also highly sable. Its E_{cell}^{ocv} only drops by 27% after 30 days (Fig. 4A, inset).

Table 1 Comparison between our glucose-powered FC with other BFCs

P_{max} (μWcm^{-2})	E_{cell}^{ocv} (V)	C (mM)	Electrode material	Reference No.
2375 ± 170	1.10	200	3D graphene-Co_3O_4 hybrid	Present
24.3 ± 4	0.58 ± 0.05	100	Graphene	40
1450 ± 240	0.80	400	Carbon fiber sheet	41
740	0.83	15	Carbon nanotube fibers	42
350	0.88	15	Carbon fibers	43
1.36	0.884	1000	Graphite plates	44
1300	0.95	50	Carbon nanotube	39

Fig. 4B presents the polarization curve (voltage-current relation with varying load resistance) and the corresponding power output, in the presence of 200 mM glucose. The slope of the linear region of the polarization curve indicates the internal resistance of the FC which is estimated to be r_i = 214 Ω based on fitting. Such small internal resistance ensures small internal energy consumption (heat generation), thus high efficiency in electricity production. When the load resistance matches the internal resistance, the maximum power output (P_{max}) is reached at ~2.38 ± 0.17 mW cm^{-2} (corresponding to unit volume power density of 47.6 mW cm^{-3} calculated according to the electrode thickness). It is superior to the previously reported results (Table 1).

The BFCs based on glucose-specific enzymes can only use glucose as the fuel while wasting other possible fuels in the biomass. Uniquely, we find that our enzyme-free FCs are able to harvest energy from other sugar molecules (specifically, disaccharide sucrose and β-lactose) in addition to glucose (monosaccharide) (Fig. 4C). Also as shown in Fig. 4C, the maximum power output (P_{max}) is fuel-concentration dependent (highest P_{max} reached at ~200 mM for glucose, ~50 mM for sucrose, and ~100 mM for β-lactose). Decrease of P_{max} at a too-high sugar concentration is presumably, at least in part, due to increase of internal resistance and decrease of diffusion process (because of increase of viscosity). Moreover, we show that the device is able to havest electricity from the mixture of three sugar species (50 mM glucose, 25 mM sucrose, and 25 mM β-lactose) and deliver an output higher than that from any individual species alone at the same concentration (100 mM) (Fig. 4). As a demonstration of its practical use, we show that two FCs in series can light up a yellow LED (turn-on voltage ~1.8 V).

Because BFCs are promsing powering uints for implanted devices due to the abundant availability of biofuels in the living systems, we examined the cytotoxicity of the 3D graphene-Co_3O_4 electrode. As shown (Fig. S4 in ESI), the hybrid electrode didn't impose appreciable cytotoxicity to the tested cell model (PC12 cells – a cell line derived from rat adrenal medulla).

Fuel cells using noble metal nanoparticles as the catalysts for glucose oxidation have been demonstrated in many studies.[45-48] But in addition to the problems that noble metal nanoparticles are expensive and prone to poisioning by the reaction intermediates, these FCs have to operate in highly basic conditions (thus often called as glucose alkaline fuel cells) and sometimes high temperature.[49, 50] In constrast, our FC using inexpensive Co_3O_4 as the catalyst can operate in mild and physiological conditions and is a superior alternative to enzymatic biofuel cells. At pH 7.0, our glucose-powered fuel cell is able to deliver a power output density of 1.55 ± 0.11 mW cm^{-2} (n = 3) which outperforms that of the previously reported BFCs and is much higher than that of all glucose alkaline fuel cells whose outputs drastically drop to a few μW cm^{-2} at neural pH.[51]

4. Conclusion

We herein demonstrate a unique fuel cell which, equipped with two identical enzyme-free electrodes based on Co_3O_4 coated 3D graphene, is able to efficiently harvest electricity from various sweet fuels (glucose, sucrose, or lactose). This development takes advantage of the fact that Co_3O_4 is a mixed valence compound, in which, the higher valence state (Co^{III}) can act as an ideal oxidation catalyst towards glucose while the lower valence state (Co^{II}) can serve as an excellent reduction catalyst towards oxygen. Using glucose as the fuel, our FC offers the highest open circuit potential and power density output ever reported. Such high performance is owing to not only the exceptional dual catalytic abilities of nanostructured Co_3O_4 but also the extraordinary properties of 3D graphene. The graphene foam provides a 3D scaffold with large surface area to support abundant Co_3O_4 catalysts, highly-conductive 3D network for rapid charge transport, and macroporous structure to ensure

unhindered diffusion of ions and substances. Finally, without the use of bioenzymes, our sugar-powered FC is of low-cost and high stability.

Acknowledgements

This work was supported by a SERC Grant (#102 170 0142) from the Agency for Science, Technology and Research (A*STAR, Singapore), an AcRF tier 2 grant (MOE2011-T2-2-010) from Ministry of Eduction (Singapore) and a Competitive Research Program grant (NRF-CRP2-2007-02) from the Singapore National Research Foundation.

Notes and References

1 M. J. Moehlenbrock and S. D. Minteer, *Chem. Soc. Rev.*, 2008, **37**, 1188-1196.

2 M. J. Cooney, V. Svoboda, C. Lau, G. Martin and S. D. Minteer, *Energy Environ. Sci.*, 2008, **1**, 320-337.

3 S. C. Barton, J. Gallaway and P. Atanassov, *Chem. Rev.*, 2004, **104**, 4867-4886.

4 X. Y. Yang, G. Tian, N. Jiang and B. L. Su, *Energy Environ. Sci.*, 2012, **5**, 5540-5563.

5 J. C. Lovett, S. Hards, J. Clancy and C. Snell, *Energy Environ. Sci.*, 2011, **4**, 261-268.

6 U. Schroder, *Angew. Chem.,-Int. Ed.*, 2012, **51**, 7370-7372.

7 A. Szczupak, J. Halamek, L. Halamkova, V. Bocharova, L. Alfonta and E. Katz, *Energy Environ. Sci.*, 2012, **5**, 8891-8895.

8 T. Miyake, K. Haneda, N. Nagai, Y. Yatagawa, H. Onami, S. Yoshino, T. Abe and M. Nishizawa, *Energy Environ. Sci.*, 2011, **4**, 5008-5012.

9 Y. Liu, M. K. Wang, F. Zhao, B. F. Liu and S. J. Dong, *Chem.-Eur. J.*, 2005, **11**, 4970-4974.

10 Z. Y. Zhou, N. Tian, J. T. Li, I. Broadwell and S. G. Sun, *Chem. Soc. Rev.*, 2011, **40**, 4167-4185.

11 X. W. Liu, D. S. Wang and Y. D. Li, *Nano Today*, 2012, **7**, 448-466.

12 J. Gu, Y. W. Zhang and F. Tao, *Chem. Soc. Rev.*, 2012, **41**, 8050-8065.

13 Y. Y. Liang, Y. G. Li, H. L. Wang, J. G. Zhou, J. Wang, T. Regier and H. J. Dai, *Nat. Mater.*, 2011, **10**, 780-786.

14 X. W. Xie, Y. Li, Z. Q. Liu, M. Haruta and W. J. Shen, *Nature*, 2009, **458**, 746-749.

15 X. W. Xie and W. J. Shen, *Nanoscale*, 2009, **1**, 50-60.

16 X. W. Wang, X. C. Dong, Y. Q. Wen, C. M. Li, Q. H. Xiong and P. Chen, *Chem. Commun.*, 2012, **48**, 6490-6492.

17 Y. Ding, Y. Wang, L. A. Su, M. Bellagamba, H. Zhang and Y. Lei, *Biosens. Bioelectron.*, 2010, **26**, 542-548.

18 C. W. Kung, C. Y. Lin, Y. H. Lai, R. Vittal and K. C. Ho, *Biosens. Bioelectron.*, 2011, **27**, 125-131.

19 B. F. Machado and P. Serp, *Catal. Sci. Technol.*, 2012, **2**, 54-75.

20 C. C. Huang, C. Li and G. Q. Shi, *Energy Environ. Sci.*, 2012, **5**, 8848-8868.

21 S. H. Hur and J.-N. Park, *Asia-Pac. J. Chem. Eng.*, 2013, doi:10.1002/apj.1676.

22 Z. H. Wen, S. Q. Ci, F. Zhang, X. L. Feng, S. M. Cui, S. Mao, S. L. Luo, Z. He and J. H. Chen, *Adv. Mater.*, 2012, **24**, 1399-1404.

23 Z. P. Chen, W. C. Ren, L. B. Gao, B. L. Liu, S. F. Pei and H. M. Cheng, *Nat. Mater.*, 2011, **10**, 424-428.

24 Y. C. Yong, X. C. Dong, M. B. Chan-Park, H. Song and P. Chen, *ACS Nano*, 2012, **6**, 2394-2400.

25 S. Nardecchia, D. Carriazo, M. L. Ferrer, M. C. Gutierrez and F. del Monte, *Chem. Soc. Rev.*, 2013, **42**, 794-830.

26 X. C. Dong, Y. W. Ma, G. Y. Zhu, Y. X. Huang, J. Wang, M. B. Chan-Park, L. H. Wang, W. Huang and P. Chen, *J. Mater. Chem.*, 2012, **22**, 17044-17048.

27 X. C. Dong, Y. F. Cao, J. Wang, M. B. Chan-Park, L. H. Wang, W. Huang and P. Chen, *RSC Adv.*, 2012, **2**, 4364-4369.

28 T. Maiyalagan, X. C. Dong, P. Chen and X. Wang, *J. Mater. Chem.*, 2012, **22**, 5286-5290.

29 X. C. Dong, B. Li, A. Wei, X. H. Cao, M. B. Chan-Park, H. Zhang, L. J. Li, W. Huang and P. Chen, *Carbon*, 2011, **49**, 2944-2949.

30 X. C. Dong, P. Wang, W. J. Fang, C. Y. Su, Y. H. Chen, L. J. Li, W. Huang and P. Chen, *Carbon*, 2011, **49**, 3672-3678.

31 D. C. Harris, *Quantitative chemical analysis, 8th ed*, W. H. Freeman and Company, New York, 2010, p. 298.

32 I. G. Casella and M. Gatta, *J. Electroanal. Chem.*, 2002, **534**, 31-38.

33 J. Yang, W. D. Zhang and S. Gunasekaran, *Electrochim. Acta*, 2011, **56**, 5538-5544.

34 M. Hamdani, R. N. Singh and P. Chartier, *Int. J. Electrochem. Sci.*, 2010, **5**, 556-577.

35 E. B. Castro, C. A. Gervasi and J. R. Vilche, *J. Appl. Electrochem.*, 1998, **28**, 835-841.

36 J. S. Mu, Y. Wang, M. Zhao and L. Zhang, *Chem. Commun.*, 2012, **48**, 2540-2542.

37 M. Pourbaix, *Atlas d'équilibres électrochimiques à 25 °C*, Gauthier-Villars, Paris, 1963, pp. 322-329.

38 J. B. Xu, P. Gao and T. S. Zhao, *Energy Environ. Sci.*, 2012, **5**, 5333-5339.

39 A. Zebda, C. Gondran, A. Le Goff, M. Holzinger, P. Cinquin and S. Cosnier, *Nat. Commun.*, 2011, **2**.

40 C. Liu, S. Alwarappan, Z. F. Chen, X. X. Kong and C. Z. Li, *Biosens. Bioelectron.*, 2010, **25**, 1829-1833.

41 H. Sakai, T. Nakagawa, Y. Tokita, T. Hatazawa, T. Ikeda, S. Tsujimura and K. Kano, *Energy Environ. Sci.*, 2009, **2**, 133-138.

42 F. Gao, L. Viry, M. Maugey, P. Poulin and N. Mano, *Nat. Commun.*, 2010, **1**.

43 V. Soukharev, N. Mano and A. Heller, *J. Am. Chem. Soc.*, 2004, **126**, 8368-8369.

44 S. Fishilevich, L. Amir, Y. Fridman, A. Aharoni and L. Alfonta, *J. Am. Chem. Soc*, 2009, **131**, 12052-12053.

45 L. Li, K. Scott and E. H. Yu, *J. Power Sources*, 2013, **221**, 1-5.

46 F. M. Cuevas-Muniz, M. Guerra-Balcazar, J. P. Esquivel, N. Sabate, L. G. Arriaga and J. Ledesma-Garcia, *J. Power Sources*, 2012, **216**, 297-303.

47 N. Fujiwara, S. Yamazaki, Z. Siroma, T. Ioroi, H. Senoh and K. Yasuda, *Electrochem. Commun.*, 2009, **11**, 390-392.

48 D. Basu and S. Basu, *Electrochim. Acta*, 2011, **56**, 6106-6113.

49 J. Y. Chen, C. X. Zhao, M. M. Zhi, K. W. Wang, L. L. Deng and G. Xu, *Electrochim. Acta*, 2012, **66**, 133-138.

50 L. An, T. S. Zhao, S. Y. Shen, Q. X. Wu and R. Chen, *J. Power Sources*, 2011, **196**, 186-190.

51 A. Kloke, C. Kohler, R. Zengerle and S. Kerzenmacher, *J. Phys. Chem. C*, 2012, **116**, 19689-19698.